

## Correlation of Thermal and Microstructural Properties of an Al-0.60wt%Mg-0.25wt%Fe-0.05wt%Cu Alloy Unidirectionally Solidified

Pedro LAMARÃO\*, Clóvis SANTANA, Kazuo KAMIZONO, Isabella JORGE, José QUARESMA

Federal University of Pará – Augusto Corrêa Str. n° 01, PO BOX 479, Belém-PA, Brazil

crossref <http://dx.doi.org/10.5755/j01.ms.20.3.5015>

Received 27 August 2013; accepted 13 December 2013

This work aims to study the thermal, mechanical and microstructural properties of an Al-0.60 wt% Mg-0.25 wt% Fe-0.05 wt% Cu alloy for application as an electrical conductor. The ingots were obtained by unidirectional horizontal casting, and were sectioned in specific positions to the production of test specimens destined to mechanical tests and microstructural characterization. As results, one can observe that it was possible to obtain experimental models of correlation between the average dimple diameters and thermal variables, demonstrating a trend on the formation of smaller fracture dimples where the cooling was more intense. As one can associate smaller dimples with greater ultimate tensile strength, it is important to understand this mechanism.

*Keywords:* aluminium alloys, growth rate, cooling rate, dimples.

### 1. INTRODUCTION

In electrical applications, the commercially pure aluminum possesses the highest electrical conductivity among aluminum conductors. Its application is only restricted due to its low strength [1]. A typical solution for this problem is the use of aluminum conductors steel reinforced (ACSR), which has a high strength core material surrounded by wires of high conductivity material. By varying the number of steel wires for a conductor of a certain cross section, one can obtain elevated tensile strength or elevated electrical conductivity, but not both at the same time [2]. This lead to the application of the lightweight precipitation hardenable Al-Mg-Si alloys (6000 series), that have better mechanical resistance than aluminum wires (approximately 300 MPa), but an electrical conductivity lower than conventional wires. The aluminum alloys based on this system gained significant interest during the last decades and are still object of study for many authors [1–5]. Also, there has been developed studies with heat-resistant materials for electrical conductors, which use elements of the group 4 (Zr, Ti, Hf) [6] or with rare earths (Sc) [7], some researchers are also developing aluminum conductors with composite cores [8].

As the cable industry uses conventional solidification to manufacture its products, it is important to study the influence of the thermal variables in transient solidification over the properties of the materials used. Hence, this paper studied an Al-0.60 wt% Mg-0.25 wt% Fe-0.05 wt% Cu alloy, which is an experimental system derived from the 6101B alloy [9], excluding Si, Mn and Zn content. The objective of this study is, therefore: Study the influence of heat transfer (for the studied alloy, under horizontal unidirectional solidification) over the tensile strength and the average dimple diameter for the fractured specimens.

### 2. EXPERIMENTAL

The alloy was prepared in a kaolin coated SiC crucible and cast on a muffle furnace at the temperature of 850 °C, followed by stirring, degassing with Ar and pouring with a superheating of 10 % in a unidirectional horizontal solidification apparatus (Fig. 1). The thermocouples were connected to an AHLBORN ALMEMO data logger, with measurements being recorded at each second.

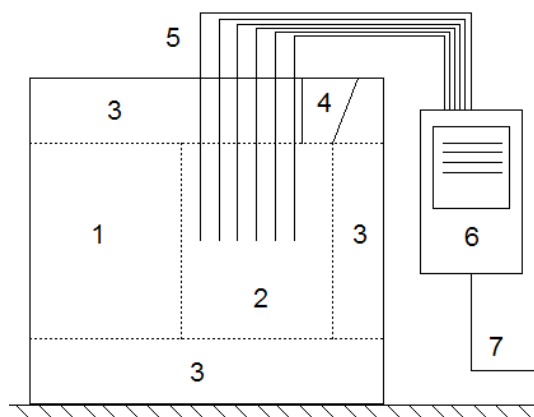


**Fig. 1.** Schematic front view of the unidirectional horizontal solidification apparatus, 1 – SAE 1010 steel mould, 2 – (60×60×110) mm casting chamber, 3 – refractory walls, 4 – pouring channel, 5 – thermocouples (positioned at 7.5, 15.0, 22.5, 30.0 and 45.0 mm from the metal/mould interface, 6 – data logger, 7 – connection to PC

The chemical composition of the alloy was analysed on an SPECTROLAB SPECTRO optical mass spectrometer. The produced ingots have the dimensions of (59×59×109) mm ±1 mm (average), showing small contraction at the upper part, were sectioned using a scissor type band saw on the relative positions of the metal/mould interface of 7.5, 22.5, 37.5 and 52.5 mm, producing (13×13×110) mm samples. These samples were machined to the diameter of 9.5 mm and cold-rolled to the diameter of

\* Corresponding author. Tel./fax.: +5591-32017325.  
E-mail address: [pedrolamarao@ufpa.br](mailto:pedrolamarao@ufpa.br) (P. Lamarão)

3.0 mm (68 % of cold-working), these samples were tested by tensile strength using a KRATOS IKLC1 machine. The microstructural analysis occurred from the evaluation of the fractures obtained by the tensile strength tests. These samples were immersed into a  $(\text{CH}_3)_2\text{CO} + \text{CH}_3\text{CH}_2\text{OH}$  solution, and cleaned on a METASOM 15 ultrasound device for 10 minutes. Next, the samples were analysed on a LEO 1430 scanning electron microscope with 20 kV and 90  $\mu\text{A}$  of electron beam, with Electrons Backscattered (EBS). One studied each of the four relative positions of the metal/mould interface (7.5, 22.5, 37.5 and 52.5 mm) and for each position it were studied two different fractured samples, obtaining four fractographs. Also, the fractographs had its dimples diameters measured at the software ImageJ. The obtained results were analysed at the R statistical software, using box-whisker plots for eliminating outliers and performing Welch two sample t-tests, following the parameters described by Peternelli and Mello [10] and the description of Spiegel for the t statistic [11].

### 3. RESULTS

#### 3.1. Thermal analysis

After obtaining the alloy liquidus temperature ( $T_L$ ) experimentally, it was possible to determine the moment it was detected by the thermocouples at each specific position. This allowed to establish distance  $x$  time relationships, which, using a regression model, lead to a  $D = k_1 t^{k_2}$  equation, being  $k_1$  and  $k_2$  constants,  $t$  is the time and  $D$  is the distance from the metal/mould interface. This relationship is shown in Fig. 2.

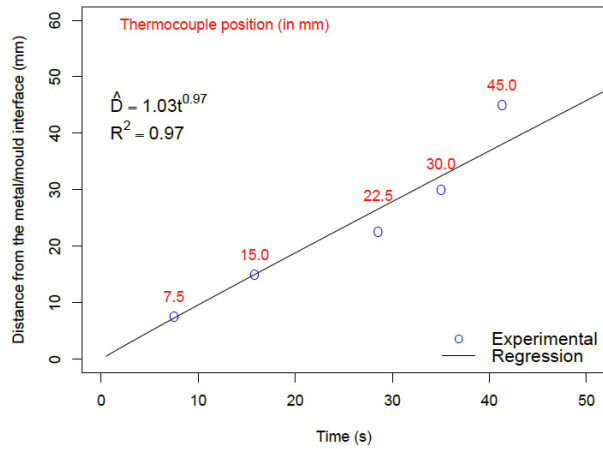


Fig. 2. Distance  $x$  time relationship

By differentiating the equation shown in Fig. 2, one can obtain the experimental growth rate (in mm/s) of the solidification process with time ( $Gr = \delta D / \delta t$ ) with a simple algebraic manipulation one can obtain the growth rate with the distance from the metal/mould interface. The analytic form of the growth rate is on Eq. 1, showing the strong dependency of this variable of the heat transfer coefficient,  $h_i$  (in  $\text{W}/\text{m}^2\text{K}$ ) during the earlier stages of solidification.  $a_s$  is the thermal diffusivity (in  $\text{m}^2/\text{s}$ ),  $\phi$  is the solid/liquid interface dislocation constant (adimensional),  $L$  is the latent heat of fusion (in  $\text{J}/\text{Kg}$ ),  $d_s$  is the density (in  $\text{Kg}/\text{m}^3$ ),  $T_f$  is the fusion temperature (in  $^\circ\text{C}$ ),  $T_0$  is the environment temperature (in  $^\circ\text{C}$ ). Fig. 3 shows the evolution of the growth rate through the ingot length

(distance from the metal/mould interface). As the solidification begins, one can observe growth values near to 0.93 mm/s. These values decrease continuously until the end of solidification, this behavior is expected due to the growth of the solidified layer, that acts as a barrier for heat transfer. Following the thermal characterization it was obtained experimentally the cooling rate ( $Cr$ ), using a method similar to the one described by Okamoto and Kishitake [12]. The relation is presented in Eq. 2, where  $Cr$  is given in  $\text{K}/\text{s}$ ,  $T_2$  is the temperature over the liquidus temperature and  $T_1$  is the temperature below it.  $t_2$  and  $t_1$  are, respectively, the times before and after the passage of  $T_L$ . Garcia [13] presents an analytic form of the cooling rate for a pure metal, which is given in Eq. 3, where it is shown its dependency on the growth rate. On the same equation,  $k_s$  is the thermal conductivity (in  $\text{W}/\text{m.K}$ ). Fig. 4 presents the cooling rate. The decreasing of the heat extraction is explained by its dependency of the growth rate and the elimination of the latent heat of fusion.

$$Gr = \frac{dD}{dt} = \left( \frac{1}{2a_s\phi} D + \frac{Ld_s}{(T_f - T_0)h_i} \right)^{-1}; \quad (1)$$

$$Cr = \frac{\bar{T}}{\bar{t}} = \frac{T_2 - T_1}{t_2 - t_1}; \quad (2)$$

$$Cr^* = \frac{d_s L}{k_s} Gr^2. \quad (3)$$

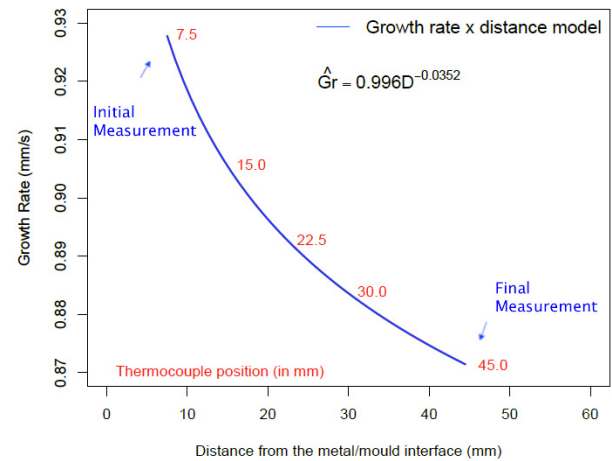


Fig. 3. Evolution of growth rate along the casting chamber length

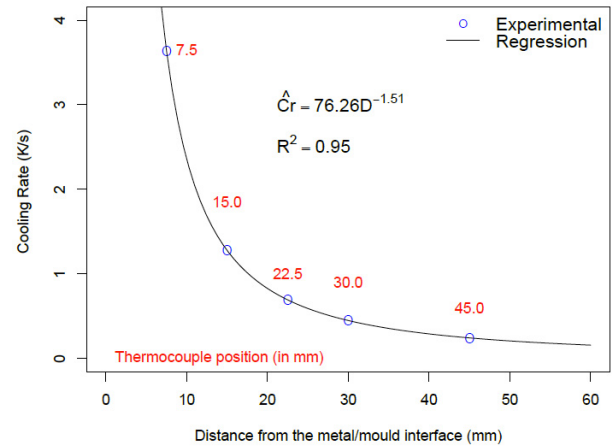
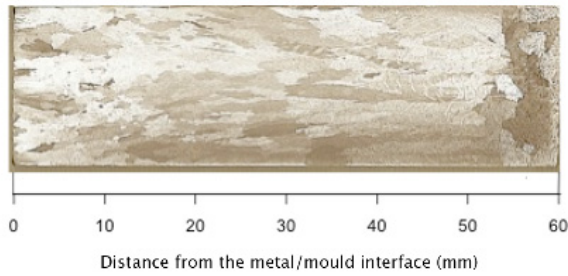


Fig. 4. Evolution of cooling rate along measurement points in the casting chamber



**Fig. 5.** As cast longitudinal solidification macrostructure after the application of a Poulton etchant (heat extraction source is on the left).

Fig. 5 is the macrostructure of an as cast longitudinal section of the solidified ingot. One applied a Poulton etchant (2 mL HF, 3 mL HCl, 20 mL HNO<sub>3</sub>, 175 mL H<sub>2</sub>O) to reveal its grained structure. The macrostructure shows that the grains near to the metal/mould interface are chilled, indicating the occurrence of intensive heat extraction. Ranging from 10 mm to 50 mm of the metal/mould interface one can observe a columnar-grained area, indicating the direction of the heat flow. The solidification process ended with the formation of equiaxed grains, as can be seen at the latest positions of the ingot.

### 3.2. Tensile strength tests

For the tensile tests, each average shown in Fig. 6 was calculated by the execution of three tests. The average standard deviations (*SD*) for each position are low, with values of 3.2 MPa. The best regression model possible is linear, showing a trend of decreasing resistance through the ingot length. This resembles the well-known Hall-Pech effect, that explains the increase of resistance of the metals as a function of the reduction of its grain size [14].

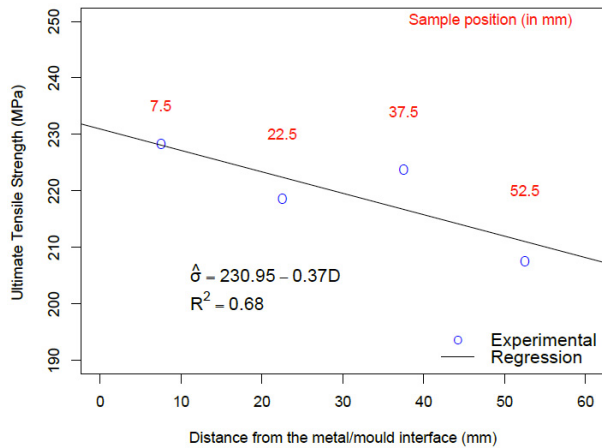


**Fig. 6.** Tensile tests results performed at four different positions along the ingot length

Other studies on the literature point to the reduction of grain size due to greater values of thermal variables as growth rate and cooling rate near to the heat extraction sources, the distance from the mold on a unidirectional solidification process can form chilled, columnar and equiaxed zones [13]. Also, the tensile tests show that, the alloy presents higher resistance than traditional aluminium wires for electrical purposes. The average value of

mechanical resistance required for 3.0 mm wires is 175 MPa [15].

### 3.3 Microstructural characterization

Measuring the fracture dimples of the tensile strength tested samples carried out the microstructural characterization. Fig. 7 shows four fractographies obtained from different positions of the ingot (7.5, 22.5, 37.5 and 52.5, respectively) these images were processed and the dimple diameters were calculated using the method described by Sharma et al. [16] as presented in Eq. 4, where  $d_1$  is the dimple length and  $d_2$  is the width. Table 1 provides the main statistical parameters of the measurements.

As one realized various measurements with different samples, it were realized histograms (Fig. 8) that indicated that the samples came from the same population, as the histograms presented good resemblance with a Gaussian distribution.

Also, it was mathematically determined whether means of sample 1 and 2 are different or not. One performed Welch two sample t-tests, as shown in Table 2. As the  $t_w$  statistics are found inside the confidence intervals established at 95 %, and the  $p$  values are greater than the significance ( $\alpha=0.05$ ), the test denies the alternative hypothesis that there are significant differences between the averages for the two samples on each position. This can be an indicative that the measurements are reliable.

$$A = \sqrt{d_1 d_2} \quad (4)$$

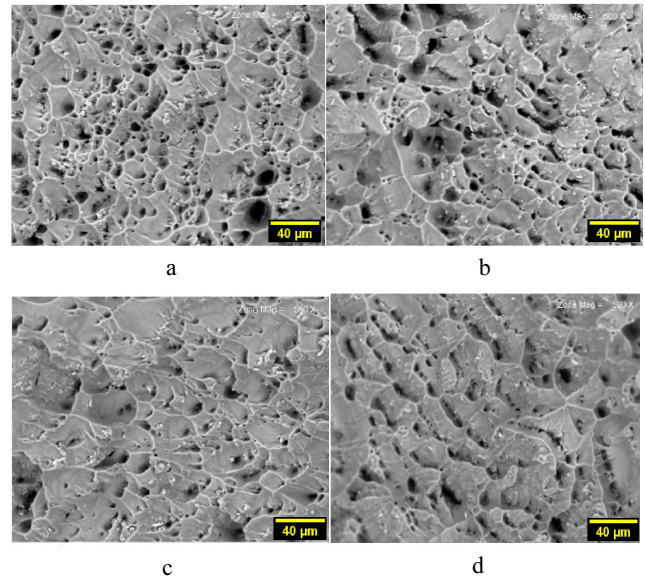


**Fig. 7.** Micrographs for the positions of (a) 7.5, (b) 22.5, (c) 37.5 and (d) 52.5 mm from the metal/mould interface

**Table 1.** Statistical parameters of the dimple measurements

Statistics	Position (mm)			
	7.5	22.5	37.5	52.5
Sample 1 (Mean), $\mu\text{m}$	15.76	16.94	21.37	20.59
Sample 2 (Mean), $\mu\text{m}$	14.70	16.79	21.25	19.87
Mean of Means, $\mu\text{m}$	15.23	16.86	21.31	20.23
Standard Deviation, $\mu\text{m}$	4.26	5.10	7.65	7.30
Range, $\mu\text{m}$	19.76	19.06	22.92	31.64

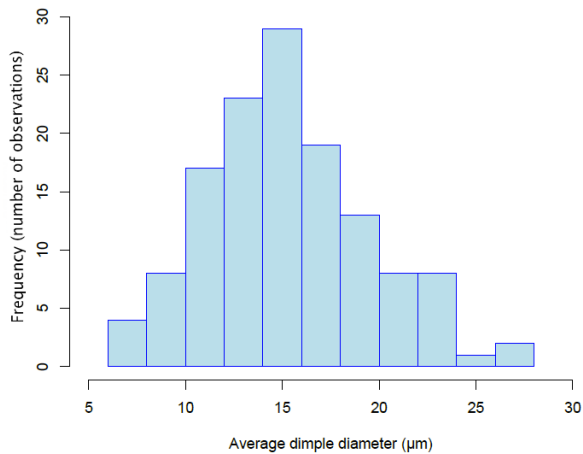


**Fig. 8.** Frequency histogram for data measured on the position of 7.5 mm

**Table 2.** Welch two-sample t-tests for differences between mean of sample 1 and sample 2

Statistics	Position (mm)			
	7.5	22.5	37.5	52.5
$t_w$	1.421	0.128	0.066	0.511
CI at 95%	[-0.17- inf.]	[-1.73- inf.]	[-2.97- inf.]	[-1.62- inf.]
$p$	0.078	0.449	0.474	0.305

Fig. 9 presents the correlation between the average dimple diameter and the growth rate, while Fig. 10 shows the correlation of the same microstructural property with the cooling rate. Both correlations obtained good  $R^2$  values, showing goodness of fit. These figures show that as the heat extraction is more intense, there is a trend to form conditions that are going to lead to fracture with smaller dimples.

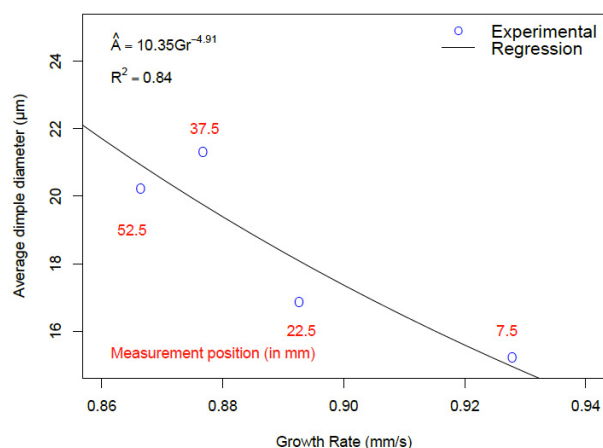


**Fig. 9.** Correlation between the average dimple diameter and growth rate

As discussed by Broek [17] inclusions like intermetallic compounds play an important role in the mechanisms that lead to the formation of dimples on ductile fracture. They are associated with the decohesion of a particle-matrix interface, during the application of a tensile stress, when the voids are extended in the same direction. This mechanism starts with void coalescence,

which is a process consisting in transition from the occurrence of diffuse plastic deformation leading the stable growth of microscopic scale internal voids to a restricted mode of plastic deformation within the ligament separating two or a row of voids [18]. In the present case, it was previously reported the presence of Fe rich particles in this alloy [19], and as the formation of  $Al_xFe_x$  aluminides has been reported to occur during solidification, predominantly the  $Al_6Fe$  at growth rates over 0.6 mm/s, as reported by Goulart et al. [20] and Allen et al. [21], this is probably the main feature associated with this mechanism.

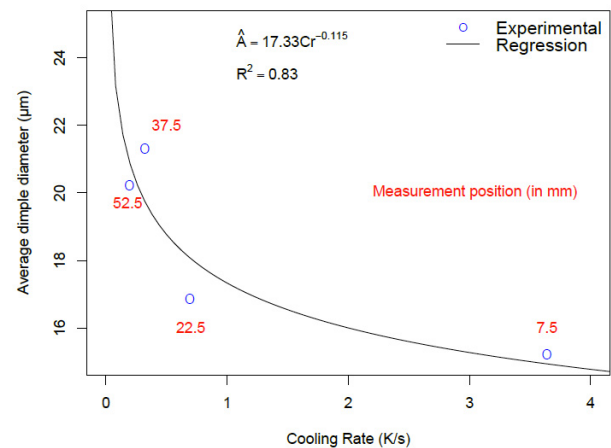


**Fig. 10.** Correlation between the average dimple diameter and cooling rate

It seems that the solute content necessary to increase void nucleation is being transported to the later positions of the ingot during solidification. This kind of segregation is expected on unidirectional solidification of binary alloys as reported in previous works in the literature [13].

## 4. CONCLUSIONS

In this research the correlation of thermal variables with the average diameter of dimples from the fractured specimens was investigated. The results showed that:

- There is good statistical correlation between the evolution of thermal variables (both growth rate ( $Gr$ ) and cooling rate ( $Cr$ )) with dimple diameters measurements;
- At greater  $Gr$  and  $Cr$ , one can observe higher values for ultimate tensile strength and smaller values for dimple diameter;
- The use of the material as an electrical conductor is suitable, because its mechanical resistance is higher than 175 MPa, which is the average value for 3.00 mm aluminium wires applied at overhead transmission lines.

## Acknowledgments

We would like to thank CAPES, CNPq and GPEMAT for the financial support and ALUBAR METAIS E CABOS for materials supply.

## REFERENCES

1. Borbuk, E. V., Murashkin, M. Y., Kazykhanov, V. U., Valiev, R. Z. Aging Behavior and Properties of Ultrafine-

- grained Aluminum Alloys of Al-Mg-Si System *Reviews on Advanced Materials Science* 31 (2) 2012: pp. 109–115.
2. **Karabay, S.** Modification of AA-6201 Alloy for Manufacturing of High Conductivity and Extra High Conductivity Wire with Property of High Tensile Stress after Artificial Aging Heat Treatment for All-aluminum Alloy Conductors *Materials and Design* 27 (10) 2006: pp. 821–832.
  3. **Martinova, Z., Damgaliev, D., Hirsh, M.** The Effect of Room Temperature Pre-aging on Tensile Strength and Electrical Properties of Thermomechanically Treated Al-Mg-Si Alloy *Journal of Mining and Metallurgy B* 38 (1–2) 2002: pp.61–73.
  4. **Smyeak, B.** Influence of Temperature and Time of Ageing on 6201 Grade AlMgSi Wire and Rod *In: 20th International Conference on Metallurgy and Materials – Metal* 5 2011, Brno, Czech Rep., Brno: VSB, 2011.
  5. **Yuan, W., Liang, Z.** Effect of Zr Addition on Properties of Al-Mg-Si Aluminum Alloy used for All-aluminum Alloy Conductors *Materials and Design* 32 (8–9) 2011: pp. 4195–4200.
  6. **Knipling, K. E., Dunand, D. C., Seidman, D. N.** Nucleation and Precipitation Strengthening in Dilute Al-Ti and Al-Zr Alloys *Metallurgical and Materials Transactions A* 38 (10) 2007: pp. 2552–2563.
  7. **Zhou, W. W., Cai, B., Li, W. J., Liu, Z. X., Yang, S.** Heat-resistant Al-0.2Sc-0.04Zr Electrical Conductor *Materials Science and Engineering A* 552 2012: pp. 353–358. <http://dx.doi.org/10.1016/j.msea.2012.05.051>
  8. **Alawar, A. A., Bosze, E. J., Nutt, S. R.** A Composite Core Conductor for Low Sag at High Temperatures *IEEE Transactions on Power Delivery* 20 (3) 2005: pp. 2193–2199.
  9. The Aluminum Association. International Alloy Designations and Chemical Composition Limits for Wrought Aluminum and Wrought Aluminum Alloys. 2009, 37 p.
  10. **Peternelli, L. A., Mello, M. P.** Conhecendo o R: Uma Visão Estatística. UFV, Viçosa, 2007.
  11. **Spiegel, M. R.** Estatística. Makron, São Paulo, 1994.
  12. **Okamoto, T., Kishitake, K.** Dendritic Structure in Unidirectionally Solidified Aluminum, Tin, and Zinc Base Binary Alloys *Journal of Crystal Growth* 29 1975: pp. 137–146,.
  13. **Garcia, A.** Solidificação: Fundamentos e Aplicações. Unicamp, Campinas, 2007.
  14. **Russel, A. M., Lee, K. L.** Structure-property Relations in Nonferrous Metals. John Wiley & Sons, New Jersey, 2005. <http://dx.doi.org/10.1002/0471708542>
  15. American Society for Testing and Materials. ASTM-B230/B 230M. Standard Specification for Aluminum 1350-H19 Wire for Electrical Purposes. West Conshohocken, 2012.
  16. **Sharma, V. M. J., Kumar, K. S., Rao, B. N., Pathak, S. D.** Effect of Microstructure and Strength on the Fracture Behavior of AA2219 Alloy *Materials Science and Engineering A* 502 (1–2) 2009: pp. 45–53.
  17. **Broek, D.** The Role of Inclusions in Ductile Fracture and Fracture Toughness *Engineering Fracture Mechanics* 5 1971: pp. 55–66.
  18. **Scheyvaerts, F., Pardoen, T., Onck, P. R.** A New Model for Void Coalescence by Internal Necking *International Journal of Damage Mechanics* 19 2010: pp. 95–126.
  19. **Lamarão, P., Santana, C., Martins, J., Quaresma, J.** Properties Correlation of an Al-Mg-Fe-Cu Alloy Unidirectionally Solidified for Overhead Transmission Lines *Metalurgia International* 18 (5) 2013: pp. 15–19.
  20. **Goulart, P. R., Spinelli, J. E., Cheung, N., Mangelinck-Nöel, N., Garcia, A.** Al-Fe Hypoeutectic Alloys Directionally Solidified Under Steady-state and Unsteady-state Conditions *Journal of Alloys and Compounds* 504 2010: pp. 205–210.
  21. **Allen, C. M., O'Reilly, K. A. Q., Cantor, B., Evans, P. V.** Intermetallic Phase Selection in 1XXX Al Alloys *Progress in Materials Science* 43 1998: pp. 89–170. [http://dx.doi.org/10.1016/S0079-6425\(98\)00003-6](http://dx.doi.org/10.1016/S0079-6425(98)00003-6)